Numerical Simulation of the Boundary-Layer Eddy Structure during the Cold-Air Outbreak of GALE IOP 2

R. I. SYKES, W. S. LEWELLEN* AND D. S. HENN

A.R.A.P. Division of California Research & Technology, Inc., Princeton, New Jersey

(Manuscript received 10 April 1989, in final form 31 July 1989)

ABSTRACT

The boundary-layer eddy structure under conditions similar to the cold-air outbreak of GALE IOP 2 is studied using numerical simulations. The simulations are run in two basic modes: a quasi-two-dimensional version that takes advantage of the observed "cloud-street" character of the flow, and a fully three-dimensional, unsteady simulation on a limited domain where periodic conditions are assumed to prevail. The two-dimensional simulation exhibits a cloud structure similar to that observed when the surface fluxes agree with the aircraft measurements. This requires very different values of effective surface roughness for temperature and humidity, which is unlikely to have been assumed in the absence of data. The three-dimensional simulation reveals that even when the eddy structure on this severely limited domain does not exhibit a dominant two-dimensional roll structure, the average turbulent statistics are quite consistent with those from the two-dimensional simulation. It is argued that a larger domain than can be readily used is needed to see a distinct cloud street pattern.

1. Introduction

An example of a classic, intense cold air outbreak occurred on 28 January 1986 during GALE IOP 2 (Mercer and Krietzberg 1986). Air temperatures were approximately 20°C colder than the sea surface temperature between the coast and the eastern edge of the Gulf Stream. Data taken during this event have been analyzed by a number of investigators (e.g., Grossman 1988; Chou and Zimmerman 1988), and probably will be well represented in this special issue. Our intent is to supply relatively high resolution numerical simulations of the boundary layer structure believed to exist under these conditions. We will rely principally upon the NCAR Electra aircraft data for establishing the conditions to be modeled.

The GOES visible image at 1800 UTC 28 January 1986 shows cloud streets to prevail over most of the experimental region. The implication of the visual observations is that the boundary layer at this time is dominated by roll vortices. Based on the assumption that this is true, we primarily use a two-dimensional model, which allows the roll vortex motion to be resolved but depends upon the turbulence closure to represent all three-dimensional motions whether they are subgrid or not. Unlike other two-dimensional roll calculations, such as Mason and Sykes (1982), Lewellen et al. (1980), Chond (1987), and Sykes et al. (1988), which have been devoted to comparing with observed spacing and turbulent statistics, our primary interest here is in simulating the cloud structures under conditions where the latent heat release should have a strong effect. Our model, detailed by Sykes et al. (1988), is reviewed in section 2. Limited results of a fully three-dimensional, large eddy simulation are also shown for comparison.

The precise boundary conditions to be used for this simulation are not known. Observations show the existence of extensive sea spray under the prevailing conditions. Although this has been the subject of much research (e.g., Bortovskii 1987) there is no precise way of specifying the surface boundary conditions for such conditions. There is a possible bias between the thermal and moisture conditions induced by the evaporation of small droplets close to the surface. Our boundary condition formulation is discussed in section 3. We examine the sensitivity of our results by a series of simulations with systematically varied surface boundary conditions.

2. Model review

Most of the results presented below were obtained using the two-dimensional model described by Sykes et al. (1988). Briefly, this is a finite-difference model with second-order accurate differencing in space and time of the incompressible, Boussinesq equations of

* Present affiliation: Dept. of Physics and Atmospheric Science, Drexel University, Philadelphia, Pennsylvania, and consultant to A.R.A.P.

Corresponding author address: Dr. W. S. Lewellen, A.R.A.P. 50 Washington Road, Princeton, NJ 08543-2229.

motion. The model is formulated using primitive variables, i.e., the three velocity components are integrated forward in time, and an elliptic equation for pressure is solved at each time step to ensure conservation of mass. The elliptic equation is solved directly using a FFT in the horizontal and line inversion in the vertical.

The thermodynamics are represented by conservation equations for liquid water potential temperature, θ_l, and total moisture content, q. These variables are chosen for their conservation properties during phase changes of water. The buoyancy of the fluid is proportional to the virtual potential temperature, θ_v, which is given by Sommeria and Deardorff (1977) as

$$\theta_v = \left[\theta_l + \frac{\theta}{T}\frac{L}{c_p} q_l\right][1 + 0.61q - 1.61q_l]$$

where q_l is the liquid water content, θ is the potential temperature, T is the actual temperature, L is the latent heat of evaporation, and c_p is the specific heat of air. We further assume that $\theta/T = e^{\kappa z/H}$, where z is the height coordinate, H is the scale height of the atmosphere, which we take to be 8 km, and $\kappa = 0.285$.

The liquid water content is calculated using the partial cloudiness formulation of Sommeria and Deardorff (1977), which requires estimates of fluctuating quantities. We solve prognostic equations for k, the turbulent kinetic energy, in addition to the temperature and humidity correlations, $\overline{\theta_l'^2}$, $\overline{q'\theta_l'}$, and $\overline{q'^2}$. Here an overbar denotes an ensemble mean, and the prime denotes fluctuation from the mean. These equations are solved together with the mean flow variable equations, using a quasi-equilibrium approximation for the turbulent fluxes. The reader is referred to Sykes et al. (1988) for details of the equations of motion.

Radiation effects have not been included. We believe that the large observed surface fluxes dominate the boundary layer development, justifying the neglect of radiation; this should be investigated further.

In order to investigate some of the three-dimensional flow structures, results from a fully three-dimensional, large eddy simulation version of the model will also be presented. This model uses the same equations of motion, and the same cloudiness parameterizations as the two-dimensional model, but is able to represent the turbulent eddies more accurately. The two models use the same turbulence closure scheme but the difference is that the turbulence length scale can be specified more freely in the three-dimensional case, where it is related to the numerical grid length. In two dimensions, the turbulence length scale must be chosen to parameterize all three-dimensional motions, and is consequently not dependent on the grid length in the same way as in a three-dimensional model. The three-dimensional model without moisture effects has been described by Sykes and Henn (1989). The turbulence length scale for the subgrid closure is also discussed there, in addition to the difference between two- and three-dimensional solutions.

3. Surface boundary conditions

The parameterization of the surface fluxes of momentum, heat and moisture is one of the most important factors determining the boundary layer development in the simulated cold-air outbreak. Various drag laws are available for calculation of the momentum exchange at the sea surface, e.g., Garrett (1977), Wu (1980), and there is some agreement with regard to the effective roughness length, z_0, or bulk transfer coefficient, c_D, as a function of wind speed. The parameterization of heat and moisture fluxes seem less certain, although the analysis of Liu et al. (1979) has received some support from field measurements. Liu et al., in arguing that the viscous sublayer plays a critical role in the determination of surface fluxes, develop a form for the bulk transfer coefficients that is consistent with Monin–Obukhov similarity theory matched to the viscous sublayer. This results in a transfer coefficient for either heat or moisture which decreases with increasing wind speed, in contrast to the momentum drag coefficient, which increases with wind speed. As noted by Liu et al., their heat and moisture coefficients should be expected to change when the air–sea interface is affected by wave breaking and there is a mixture of air bubbles in the sea and water droplets in the air.

The aircraft data from GALE IOP 2 contain direct measurements of the turbulent fluxes in addition to the sea surface temperature and mean air temperature and humidity. The aircraft flew a number of "stacks" consisting of several horizontal flight legs at different altitudes over a fixed position. The relevant quantities from stacks 1–3, as presented by Grossman (1988), are reproduced in Table 1, which also shows calculated values of the ratio of the bulk transfer coefficients for heat and moisture, c_H and c_E respectively, and the Bowen ratio, B. The bulk transfer coefficients are defined as

$$c_H = -\frac{\overline{w'\theta_s'}}{u(T - T_s)}$$

$$c_E = -\frac{\overline{w'q_s'}}{u(q - q_s)}$$

where the subscript, s, refers to a surface value, and the unsubscripted variables refer to the values in the atmosphere at the reference height. The surface humidity, q_s, is assumed to be the saturated humidity at the surface temperature. The Bowen ratio is defined as

$$B = \frac{\overline{w'\theta_s'}}{(L/c_p)\overline{w'q_s'}}.$$

The near-surface aircraft data were taken at a height of roughly 40 m, and we have used the measured fluxes in place of the surface fluxes in the above definitions in calculating the ratios for Table 1.

Table 1 shows that the ratio of c_H to c_E is significantly less than 1, i.e., under the meteorological conditions

TABLE 1. IOP 2 observations from Grossman (1988).

	Stack 1	Stack 2	Stack 3
Distance offshore (km)	55	108	179
Time of observation (UTC)	2030	1930	1800
SST (°C)	13.1	18.6	21.5
$\overline{w'\theta'_s}$ (°C m s^{-1})	0.174	0.285	0.280
$\overline{w'q'_s}$ (m s^{-1} g kg^{-1})	0.113	0.238	0.261
c_H/c_E	0.62	0.55	0.69
Bowen ratio, B	0.62	0.48	0.43
Near surface			
u (m s^{-1})	7.8	9.7	11.1
θ (°C)	−8.7	−5.7	1.1
q (g kg^{-1})	1.17	1.75	2.42
Cloud base (m)	N/A	500	300
Cloud top (m)	N/A	1200	1800

of IOP 2, moisture transfer appears to be more efficient than sensible heat transfer. In contrast, the formulation of Liu et al. yields a ratio of c_H/c_E which is approximately 1 for wind speeds between 10 and 20 m s^{-1}. The fluxes and Bowen ratio resulting from different transfer coefficients may be expected to have a strong influence on the boundary layer structure. Grossman reports the occurrence of "sea-smoke," rising plumes of liquid water from the surface, over the Gulf Stream at the time of the aircraft flights. We shall show that such phenomena are consistent with numerical simulations using the observed surface fluxes, further confirming the significant difference between heat and moisture transfer during IOP 2.

The model boundary conditions are implemented through Monin–Obukhov similarity functions, which give the relationship between the mean profile and the surface flux of any conserved quantity. The effective transfer coefficient in this formulation is a function of stability and the surface roughness associated with the appropriate variable, i.e., momentum, liquid water potential temperature, or moisture. The input requirements for this formulation are therefore the surface value of the variable and the roughness length; the stability is determined by the model calculations. Momentum is taken to be zero at the surface and the surface humidity is assumed to be the saturated value, i.e., it is a function of surface temperature only. The surface value of θ_l is specified uniformly as the observed actual sea-surface temperature, which varies with distance offshore; we assume here that $\theta_{l_s} = T_s$, i.e., no liquid water at the surface. Although we shall present model calculations indicating the presence of liquid water at the lowest model grid-level, the numerical magnitudes are small enough to justify this assumption. For the momentum roughness, z_0, we use the parameterization due to Charnock (1955), which can be written as

$$z_0 = 0.0016u_*^2$$

where u_* is the surface friction velocity in m s^{-1}, and z_0 is in meters. With z_0 and the sea surface temperature given, we have made adjustments to the temperature roughness, z_T, and humidity roughness, z_q, until the model-predicted surface fluxes were in reasonable agreement with the observations. Our principal comparison with the observations is based on this adjustment; however, we shall also present some sensitivity studies to illustrate the effects of variation in surface boundary conditions.

4. Description of model integrations

The equations of motion are integrated forward in time in a periodic domain. There are no variations in the x-direction in the two-dimensional integrations. The model is driven by time-varying, uniform surface boundary conditions and a geostrophic wind of 15 m s^{-1} directed 10° to the right of the x-axis. In comparing with observations, we are assuming that the time-dependent integrations in our fixed domain are equivalent to translating with a fixed speed over a steady, spatially varying surface. Thus, we are considering the idealized steady-state problem of a wind blowing nearly directly offshore from an infinite straight coastline over an ocean with surface temperature varying normal to the coast, but uniform parallel to the coast, i.e., along the y-axis. With an average boundary layer wind speed in the x-direction of about 13 m s^{-1}, stacks 1, 2 and 3 correspond roughly with 4200 s, 8400 s and 13 800 s in the model integrations. The wind speeds in the calculation are somewhat higher than the observed values in the lower boundary layer, although there is an observation of 16 m s^{-1} at the top of the mixed layer. We do not believe that the boundary layer structure depends strongly on the wind speed, however, except that the transit time between stacks is proportional to wind speed.

As indicated in Table 1, the aircraft sampled the air at stacks 1, 2, and 3 in reverse order, i.e., the upwind stack was sampled last. Unfortunately, the conditions are not completely stationary during the approximately three hours of the observations; there is some temporal diminishing of the wind speed and warming of the atmosphere during this period. Consequently, neither the measurements nor the model calculation accurately follow an air parcel through its development off shore.

The initial wind profile is obtained by running a one-dimensional, dry version of the model to steady

TABLE 2. Vertical grid spacing.

Grid 1		Grid 2		Grid 3	
Z	ΔZ	Z	ΔZ	Z	ΔZ
0	20	0	30	0	40
500	75	700	100	825	75
1000	30	1400	40	1800	50
1300	30	1800	40	2500	50
5000	500	6000	500	6000	500
8500	500	8500	500	8500	500

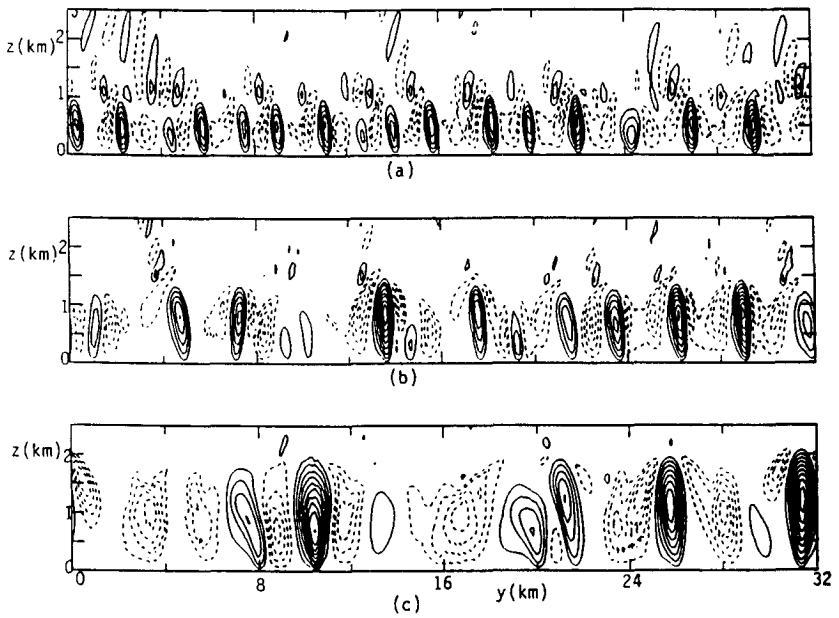

FIG. 1. Vertical velocity field from the two-dimensional model. Contour interval is 0.5 m s^{-1}; dashed lines denote negative values, zero contour omitted. (a) t = 4200 s (stack 1); (b) 8400 s (stack 2); (c) 13 800 s (stack 3).

state, with no heat flux, giving a near-equilibrium Ekman layer. The initial θ_l-profile is specified by a constant value of −8°C below the inversion at 600 m and a constant gradient of 0.0075°C m^{-1} above. Likewise, the initial humidity profile is specified by a constant value of 1 g kg^{-1} below the inversion and a constant relative humidity of 0.4 above. Since no measurements are available at the coast, we have adjusted the initial mixed-layer values of temperature and humidity by trial-and-error so that the two-dimensional integrations at 4200 and 8400 s are in close agreement with the observed temperature and humidity at stacks 1 and 2.

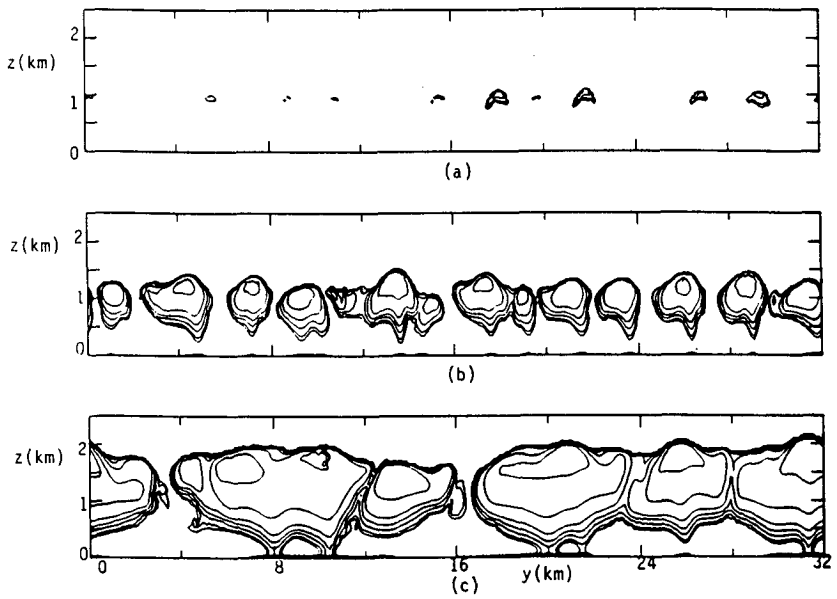

FIG. 2. Liquid water field from the two-dimensional integration. Contour levels are 0.01, 0.02, 0.05, 0.1, 0.2, 0.5, 1.0 g kg^{-1}. (a) t = 4200 s (stack 1); (b) t = 8400 s (stack 2); (c) t = 13 800 s (stack 3).

The initial solution is perturbed in two or three dimensions by a random vertical velocity field with amplitudes of a few centimeters per second. The surface temperature is specified using the values in Table 1, with a constant temperature assumed from the coast to stack 1 (0 to 4200 s) and linear interpolation used between times corresponding to the stacks. We prefer to compute the boundary layer development out to stack 1 rather than initialize at that location, since the convective eddies require a time of roughly 2000 s to grow to finite amplitude. If this growth occurs ahead of stack 1, then the rest of the boundary layer development is computed with fully developed convection.

The grid for the two-dimensional integrations is 32 km wide and 8.5 km high with 256 uniformly distributed points in the horizontal. A nonuniform grid with 62 points is used in the vertical, with highest resolution near the surface and in the inversion region. To maintain good resolution as the boundary layer grows from 600 to 2000 m, we interpolate the fields from one grid onto another grid when the inversion exceeds a certain height. Three vertical grids are used, with the interpolations occurring at around 8000 s and 13 000 s. The grid spacing at several heights are given in Table 2. The grid for the three-dimensional integration is 6 km square with 48 points in both horizontal direction. Vertical grids with similar resolution (and grid interpolation) as in the two-dimensional integrations are used, although only 48 points are used and the height is 4.5 km.

The maximum turbulence length scale is specified as $0.075z_i$, where z_i is the average mixed layer depth;

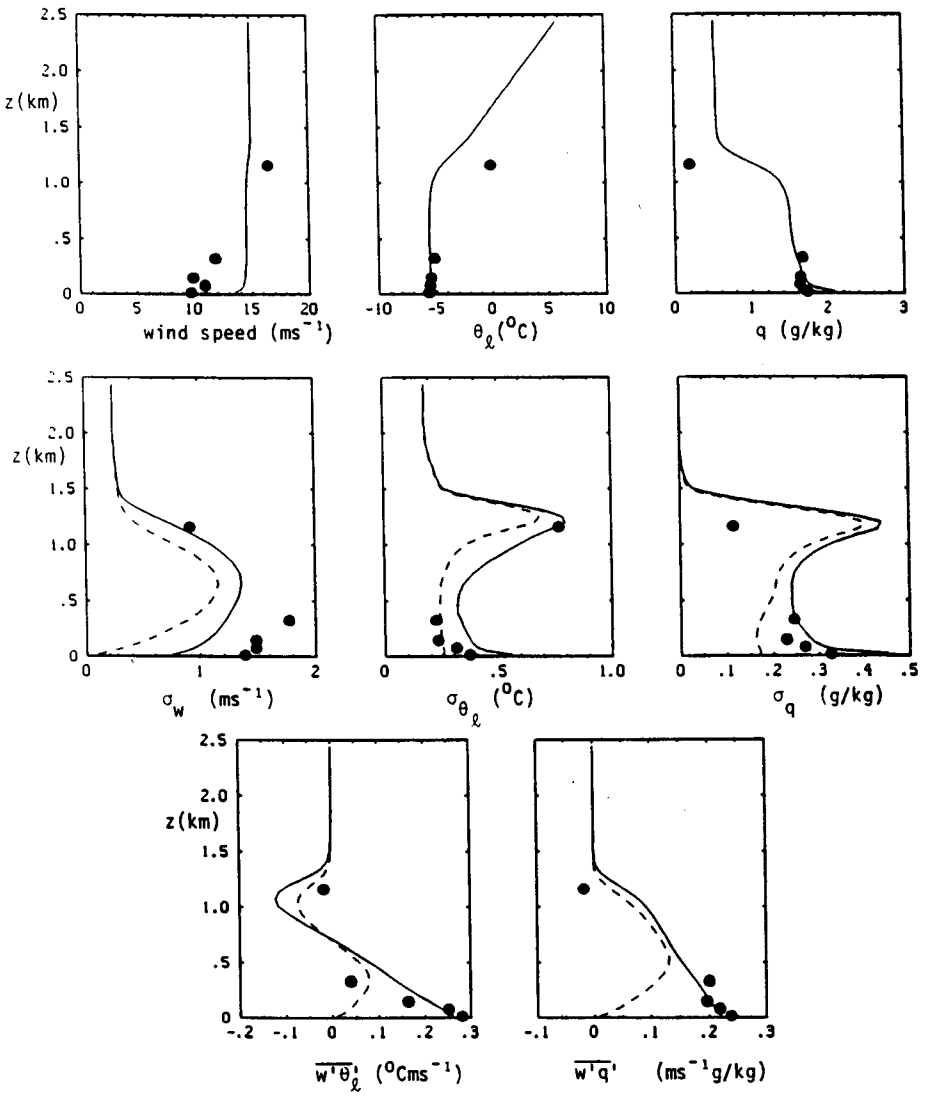

FIG. 3. Profiles at stack 2 from the two-dimensional integration. Resolved turbulence components are dashed, total is shown solid. Observations (Grossman 1988) are plotted as solid circles.

this was determined to give a reasonable partition between resolved and parameterized eddies by Sykes et al. (1988). As discussed in section 2, the turbulence lengthscale in three dimensions can be related to the grid size, and we have determined that 50 m gives a reasonable partition between resolved and parameterized turbulence for this grid. Sykes and Henn (1989) discuss the sensitivity to variation in lengthscale for a dry convective flow.

5. Comparison with observations

The development of the vertical velocity field is shown in Fig. 1. The initial roll spacing of about 2 km increases dramatically over the course of the run, until the spacing between updrafts is roughly 8 km at the end, when the convection depth is about 2 km. Figure 2 shows the liquid water field from the run, illustrating the initiation of a cloud deck after about 4000 s, i.e., beyond stack 1. The cloud layer thickens quite rapidly, and forms a near-solid layer by the end of the run. The cloud top heights appear quite consistent with Grossman's observations. The cloud formation is also accompanied by near-surface condensation at stacks 2 and 3. The vertical plumes of liquid water are carried from the surface into the cloud at stack 3. We associate these liquid water plumes with the observations of "seasmoke" described by Grossman.

The primary variables and some turbulence statistics from the two-dimensional integration are compared with the observations at stack 2 in Fig. 3. We do not show statistics at stack 3 since the observations only extend about 200 m above the surface, and therefore provide less quantitative information about the structure of the boundary layer at that station. The general agreement between the observed rms fluctuations and the predicted values is largely a result of matching the surface fluxes. The matching was achieved by using a temperature roughness length of 2×10^{-10} m, and a humidity roughness length of 10^{-5} m; the momentum roughness length is roughly 5×10^{-4} m at the wind speeds used here. This contrast between the effective thermal and moisture surface conditions is examined in section 5. The observed temperature variable was θ, the potential temperature, while our model statistics use θ_l; however, the aircraft data were mostly taken outside the cloud layer, and therefore we believe the difference should be relatively small. The discrepancy in the heat flux at the highest observation point on stack 2 may be a result of moisture effects.

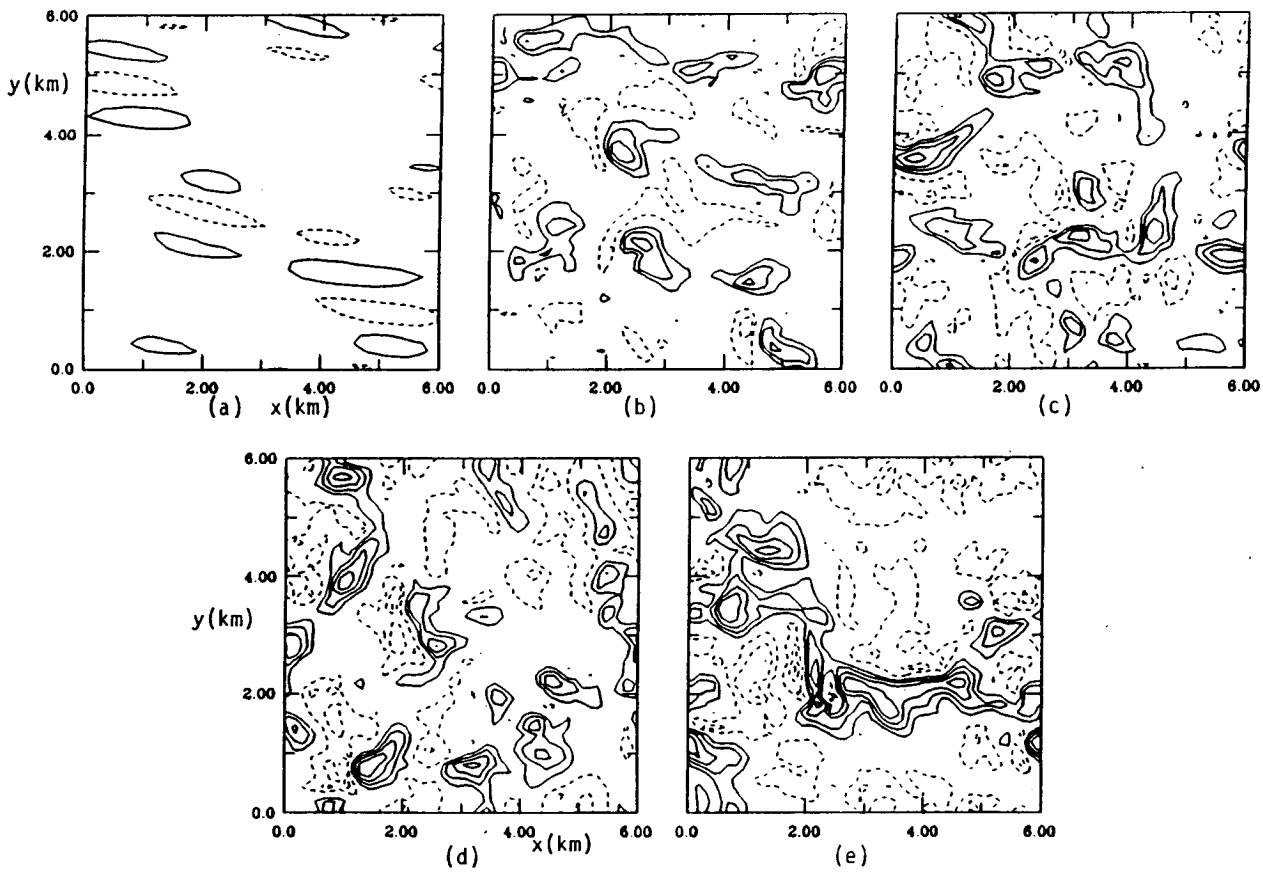

FIG. 4. Vertical velocity field at $z = 500$ m from the three-dimensional integration. Contour interval 1 m s^{-1}. (a) $t = 2100$ s; (b) $t = 4200$ s; (c) $t = 6300$ s; (d) $t = 8400$ s; (e) $t = 10\,500$ s.

There are some discrepancies between the observations and the simulated results. The wind speed observations suggest some thermal wind effect that has not been included in the simulation and there seems to be an underprediction of $\overline{w'^2}$ together with some overprediction of $\overline{\theta_l'^2}$ and $\overline{q'^2}$. It is not apparent what model changes would provide a consistent match with all the data. An increase in surface heat flux would increase $\overline{w'^2}$ but also increase $\overline{\theta_l'^2}$. An increase in effective surface roughness for momentum transport would increase $\overline{w'^2}$ and decrease both $\overline{\theta_l'^2}$ and $\overline{q'^2}$, but we were reluctant to increase z_0 much above its generally accepted range.

We now examine the results from the three-dimensional model. As noted in section 3, the three-dimensional integration used a similar vertical resolution to that used in the two-dimensional integration but the horizontal domain is 6 km × 6 km. The development of the vertical velocity field at z = 500 m is shown in Fig. 4. The initial development is seen to be in the form of elongated updrafts, which seem to break up rapidly after full amplitude is reached. There is some evidence of the 2 km wide rolls at 4200 s, but at later times the scale is much larger and no roll structure is visible. The liquid water field at z = 1000 m is shown in Fig. 5. The layer begins to develop around t = 4200 s, and thickens to form a near-solid layer by t = 8400 s. There is very little evidence of any roll structure in these fields; we speculate that any two-dimensional organization must be occurring on a larger scale, and would need an integration domain of at least 24 km to be made visible.

Despite the lack of any apparent two-dimensional organization in the three-dimensional simulation results at times corresponding to stack 2, the turbulent statistics obtained from the two-dimensional and three-dimensional simulations are quite similar, as seen in Fig. 6. The agreement is mainly due to the choice of a turbulent length scale for the two-dimensional simulation that effectively parameterizes the three-dimensional turbulence, as discussed in Sykes and Henn (1989). The main differences appear in the inversion region. The three-dimensional simulation shows increased turbulent fluctuations and entrainment fluxes, resulting in a somewhat deeper boundary layer.

Liquid water contours at low level (50 m) are shown in Fig. 7 for a limited domain in the vicinity of stack 2 from the three-dimensional simulations. There is a subtle hint of the two-dimensional structure apparent in the three-dimensional results. The sea smoke col-

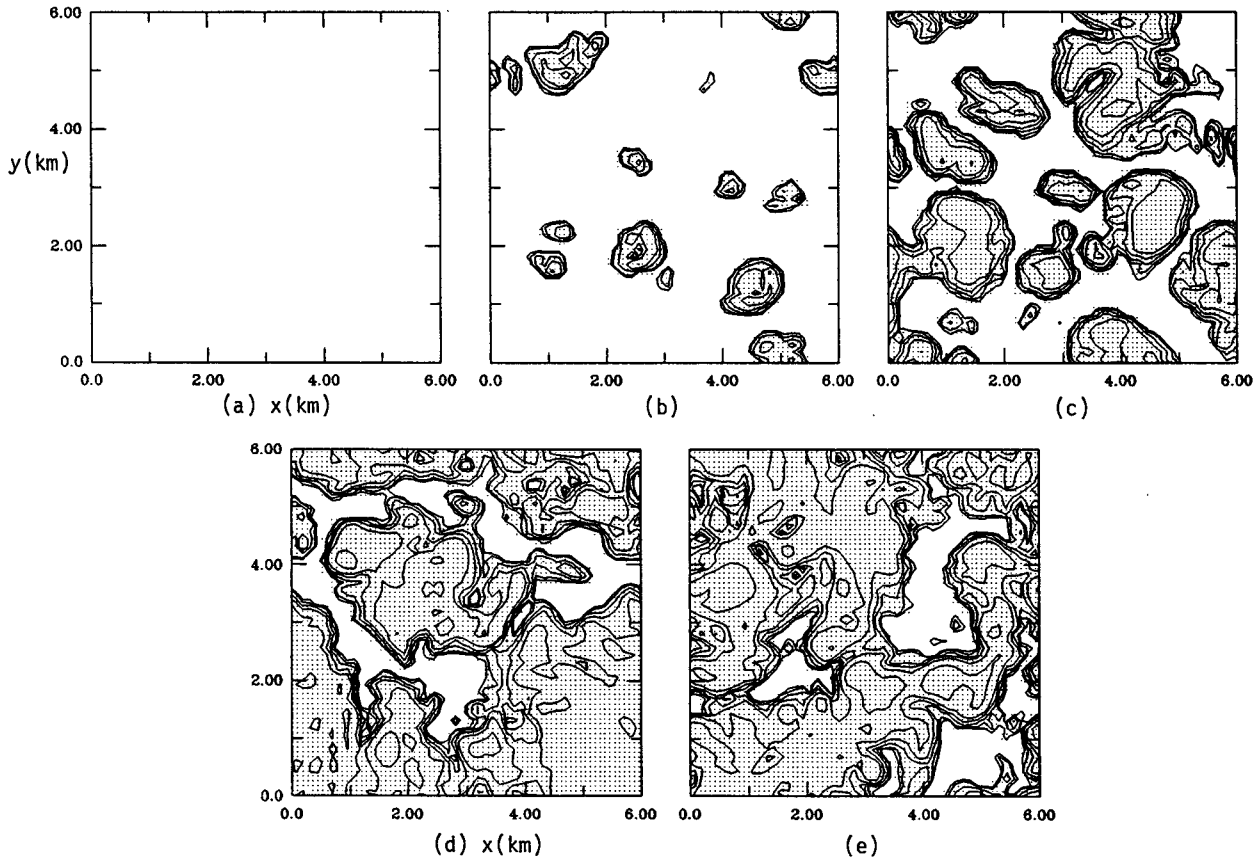

FIG. 5. Liquid water field at z = 1000 m from the three-dimensional integration. Contours as in Fig. 2. Times as in Fig. 4.

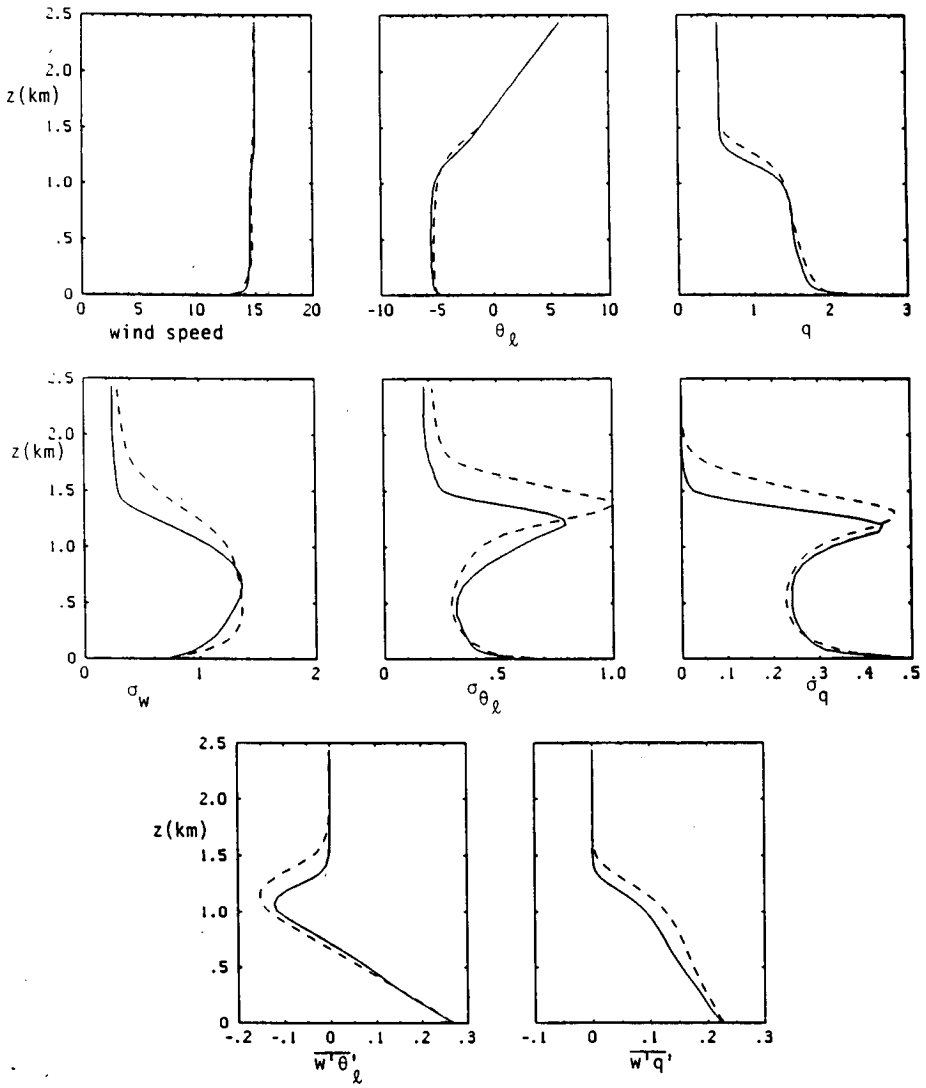

FIG. 6. Profiles at stack 2 from the three-dimensional integration (shown dashed) compared with the two-dimensional results (solid). Units as in Fig. 3.

umns are nearly lined up with the roughly 2.5 km spacing evident in the surface liquid water contours in Fig. 2. This picture is not an accurate representation of what might have been observed at a specific time. The liquid water structure was probably on a finer scale than could be resolved by the 125 m horizontal spacing of this simulation. This means that the fine scale structure is buried within the partial cloudiness fomulation. By including the partial cloudiness formulation, however, both the two-dimensional and three-dimensional models produce low level condensed water in amounts consistent with the observations of sea smoke.

We recognize that too large a dependence on the subgrid partial cloudiness parameterization could compromise the validity of the simulation. Randall (1987) has demonstrated that when the updraft fraction is significantly less than one-half and the updrafts are assumed to be cloudy while the downdrafts are clear, then the Sommeria–Deardorff formulation for the relation between the buoyancy flux and fluxes of the conserved thermodynamic variables is wrong. This may have some influence on our simulation close to the surface and at cloud top, but over the bulk of the boundary layer our resolution should be adequate to assure that updrafts are not restricted to much less than one-half of a local cell volume.

6. Sensitivity to asymmetries between temperature and humidity surface conditions

In order to approximate the surface flux conditions reported from the aircraft flights we need to use an

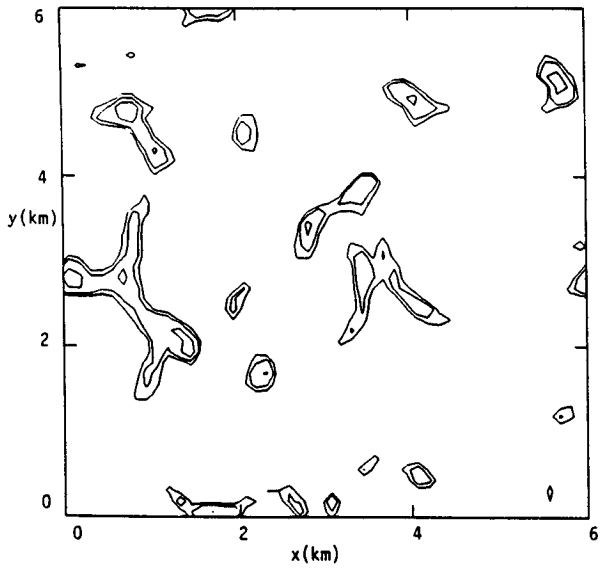

FIG. 7. Liquid water field at z = 50 m at stack 2 from the three-dimensional integration. Contours as in Fig. 2.

effective surface roughness for sensible heat which is 5 $\times 10^4$ smaller than that used for moisture. We believe this reflects the existence of sea spray in the atmospheric surface layer. Under such conditions the turbulent fluxes of heat and moisture within the surface layer are not conserved in the general manner assumed for the usual surface layer formulation involving the Monin–Obukhov stability functions and $\ln(z/z_0)$. The sea spray can provide an extra source of moisture and either a source or sink of sensible heat. It particular, when the spray droplets are predominantly small, Bortkovskii (1987) shows that they act as a significant sink for sensible heat and as a source for moisture as they are evaporated.

Our lowest grid point, at z = 10 m, is expected to be well above the sea spray layer. Thus, the usual constant flux relations should hold here, but sea spray must be accounted for in connecting these relations to the surface fluxes. We choose to do this by lumping the effects of sea spray into the surface roughness for temperature and for water vapor. We might have used a boundary condition that permitted supersaturation at the surface. However, since the appropriate degree of supersaturation is unknown, there appears to be no advantage. We have carried out a series of runs at different ratios of z_T/z_q. These might also be interpreted in terms of a sea surface saturation different from 100% if z_T/z_q is taken as equal to 1.

Figures 8 and 9 show the results of a two-dimensional run with $z_T = z_q = 2 \times 10^{-6}$ m, close to the values expected from Liu et al. (1979). Although they clearly stated that sea spray conditions would be outside the conditions used in their derivation, their formulation is often used for moderately high wind speeds. The additional heat flux (0.4 vs 0.26°C m s^{-1}) and slightly reduced moisture flux (0.21 vs 0.22 m s^{-1} g kg^{-1}) leads to reduced cloudiness in the boundary layer. The cloud base is higher at stack 3 by approximately 300 m, and all traces of any low level sea-smoke have vanished. Also, the cloud top inversion height is raised slightly by the increase in total surface heat flux. Overall, Fig. 2 appears to be more in agreement with the reported

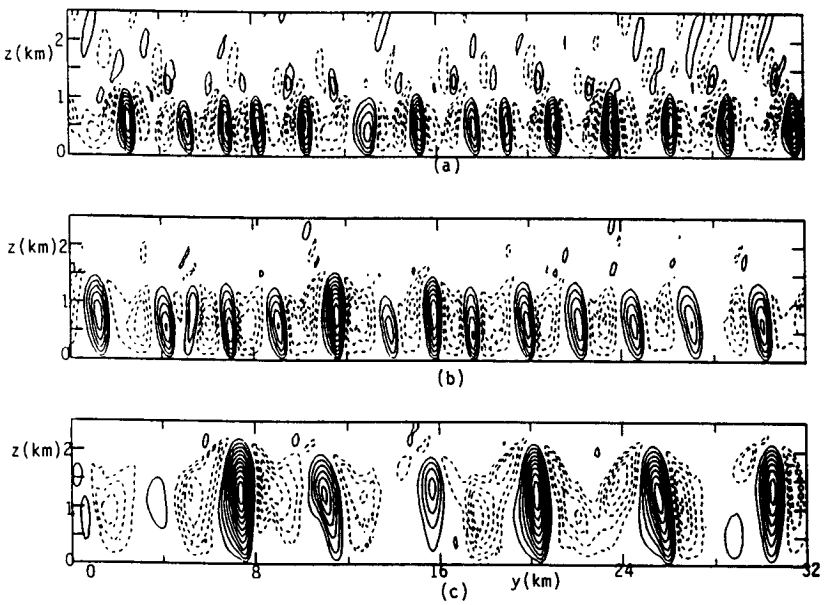

FIG. 8. Vertical velocity field from the two-dimensional integration with $z_T = z_q$ = 2×10^{-6} m. Contours as in Fig. 1. (a) stack 1; (b) stack 2; (c) stack 3.

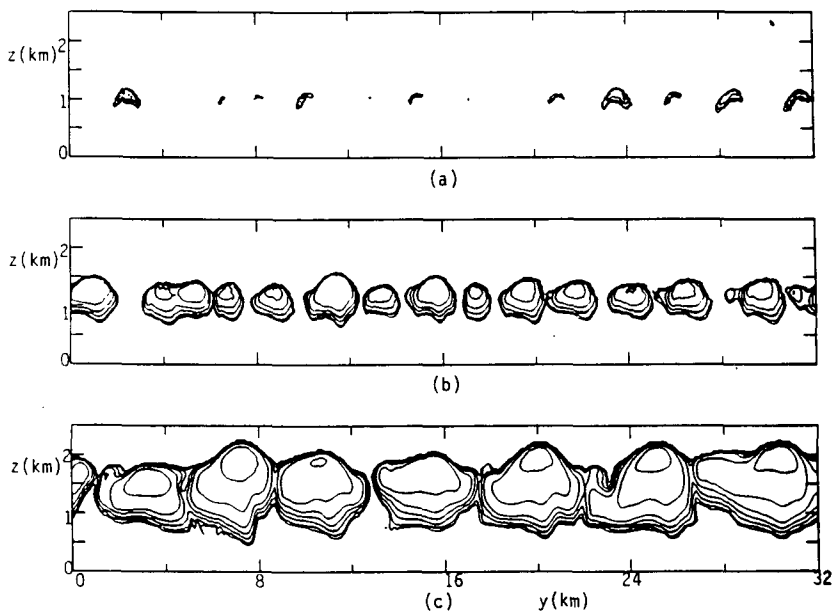

FIG. 9. Liquid water field for the run in Fig. 8. Contours as in Fig. 2.

observations of the cloud structure than is Fig. 9. Although this simulation does produce $\overline{w'^2}$ statistics somewhat closer to the reported values at stack 2, we believe that most of the aircraft turbulence data and the cloud observations are more consistent with a much larger ratio of z_T/z_q than would be indicated for this wind speed from Liu et al.'s formulation.

It is interesting to note that if 2×10^{-6} m were accepted as the appropriate effective surface roughness for the conserved thermodynamic variables, then results similar to our nominal run would imply a supersaturation level of about 25%.

The Bowen ratio for our nominal run ($\sim$0.5) is significantly lower than that obtained for the run with $z_T/z_q = 1$ ($\sim$0.75). In fact, variation of the Bowen ratio may provide a useful means of investigating the sensitivity of the boundary layer cloud structure to surface conditions. Figure 10 provides the results of a systematic variation in Bowen ratio for which the total heat flux is somewhat smaller than that of our nominal conditions. For these runs, the surface fluxes of sensible heat and humidity were simply fixed in time and space, with the total heat flux, $\overline{w'\theta'} + L/c_p\overline{w'q'}$, equal to 0.68°C m s^{-1}. Figure 10 shows that the boundary layer cloudiness is reduced as the Bowen ratio is increased. No liquid water appears in the surface layer for $B = 0.6$, but cloud columns connecting the surface with the cloud base are well established for $B = 0.4$. This is consistent with the observation of some liquid water in the surface layer for our nominal run shown in Fig. 2, which had $B \approx 0.5$.

The results of this series of runs with variable Bowen ratio are somewhat different than if a one-dimensional surface layer analysis is carried out for fixed surface fluxes at fixed temperature and humidity. When the fog analysis of Oliver et al. (1978) is interpreted in terms of the Bowen ratio, it shows surface fog should occur when $B \geqslant 0.5$ for the surface conditions under present consideration. This at first appears to be in direct conflict with the results of our present analysis of the sensitivity of the boundary layer cloudiness to Bowen ratio. The principal difference in these two analyses is that the more humid surface layer conditions appear at opposite ends of the Bowen ratio scale. When the initial conditions are specified as in our current series, decreasing B increases the humidity in the surface layer at subsequent times. Thus, an upper bound on B that will permit surface-layer liquid water is established. The surface layer analysis, however, is a local analysis, independent of initial conditions. The surface roughness for temperature and humidity are implied equal by the assumption of local similarity in their turbulent distributions for constant fluxes of each. Under these conditions, decreasing B means the surface layer humidity must decrease at a faster rate with height in order to support the decreased B, and a lower bound on B is established for conditions leading to liquid water in the surface layer.

7. Concluding remarks

Two-dimensional simulations of the boundary layer eddy structure under conditions approximating those of the cold-air outbreak of GALE IOP 2 exhibit a cloud structure similar to that observed when the surface fluxes agree with the aircraft measurements. This re-

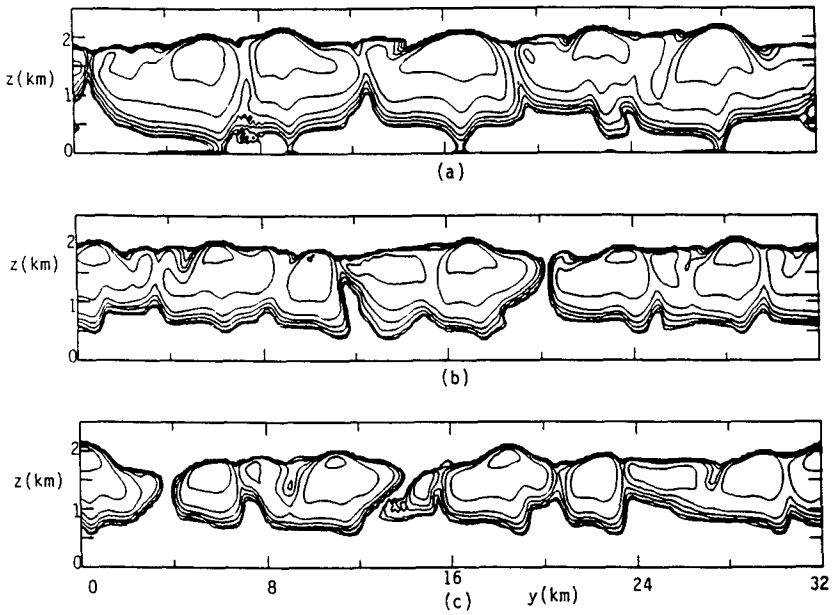

FIG. 10. Liquid water field at stack 2 from the two-dimensional integrations with varying Bowen ratio. Contours as in Fig. 2. Bowen ratio = (a) 0.4; (b) 0.6; (c) 0.8.

quires a bias between the thermal and moisture sea-surface boundary conditions that is unlikely to have been assumed in the absence of data. We interpret this bias to be the reflection of the probable existence of a sea spray layer that acts as a sink for sensible heat and a source for moisture as small droplets are evaporated close to the surface.

The results of a three-dimensional simulation are less conclusive. There is general agreement between the average variables and the turbulent statistics obtained from the three-dimensional and two-dimensional simulations, but the cloud spatial structure is different. The two-dimensional simulation naturally imposes an essential roll structure and forces the clouds into cloud streets. This is consistent with the cloud streets observed on the GOES visible image over the domain at this time. The three-dimensional simulation shows little tendency for cloud street structure. In fact, as the clouds evolve they appear to prefer a local three-dimensional structure that destroys the dominant roll structure evident in the vertical velocity distributions of the three-dimensional simulation at earlier times. Thus, the two-dimensional results actually appear closer to the observations than do the three-dimensional results. We do not have a good explanation for this. We only suggest that the actual two-dimensional organization present in the observations may be on a slightly larger scale than is permitted in the 6 km periodic domain imposed on the three-dimensional simulation. Boers et al. (1988) show an example of a visual cloud image that shows strong evidence of alignment in the direction of the wind when a domain of approximately 50 × 100 km is viewed but virtually disappears when a typical 11.5 × 11.5 km section is examined in detail. This, in spite of the fact that the peak horizontal wavelength in their data was 4.5 km. Perhaps it is fair to conclude that more than 2.5 times the dominant desired wavelength must be permitted in the three-dimensional simulation before it can exhibit that two-dimensional structure.

Acknowledgments. This research was supported by the U.S. Office of Naval Research with R. F. Abbey as Technical Monitor.

REFERENCES

Boers, R. J., J. D. Spinhirne and W. D. Hart, 1988: Lidar observations of the fine-scale variability of marine stratocumulus clouds. *J. Appl. Meteor.*, **27**, 797–810.

Bortkovskii, R. S., 1987: *Air–Sea Exchange of Heat and Moisture during Storms,* D. Reidel, 194 pp.

Charnock, H., 1955: Wind stress on a water surface. *Quart. J. Roy. Meteor. Soc.*, **81**, 369–640.

Chond, A., 1987: A numerical study of horizontal roll vortices in neutral and unstable atmospheric boundary layers. *Contrib. Atmos. Phys.*, **60**, 144–168.

Chou, S. H., and J. Zimmerman, 1988: Heat transport in the marine atmospheric boundary layer during an intense cold air outbreak, Preprints, *Seventh Conf. on Ocean–Atmospheric Interactions,* Anaheim, Amer. Meteor. Soc., 19–22.

Garrett, A. J., 1977: Review of drag coefficients over oceans and continents. *Mon. Wea. Rev.*, **105**, 915–929.

Grossman, R. L., 1988: Boundary layer warming by condensation: air-sea interaction during an extreme cold air outbreak from the eastern coast of the United States, Preprints, *Seventh Conf. on Ocean–Atmospheric Interaction,* Anaheim, Amer. Meteor. Soc., 14–18.

Lewellen, W. S., M. E. Teske and Y. P. Sheng, 1980: Micrometeorological applications of a second-order closure model of turbulent transport, *Turbulent Shear Flows 2,* Springer-Verlag; 2nd Int. Symp. on Turbulent Shear Flows, London, 366–378.

Liu, W. T., K. B. Katsaros and J. A. Businer, 1979: Bulk parameterization of air–sea exchanges of heat and water vapor including the molecular constraints at the interface. *J. Atmos. Sci.,* **36,** 1722–1735.

Mason, P. J., and R. I. Sykes, 1982: A two-dimensional numerical study of horizontal roll vortices in an inversion capped planetary boundary layer. *Quart. J. Roy. Meteor. Soc.,* **108,** 801–823.

Mercer, T. J., and C. W. Kreitzberg, 1986: *GALE Field Program Summary,* 291 pp. [Available from Dept. of Physics and Atmospheric Sciences, Drexel University, Philadelphia, PA, 19104.]

Oliver, D. A., W. S. Lewellen and G. G. Williamson, 1978: The interaction between turbulent and radiative transport in the development of fog and low-level stratus. *J. Atmos. Sci.,* **35,** 301–316.

Randall, D. A., 1987: Turbulent fluxes of liquid water and buoyancy in partly cloudy layers. *J. Atmos. Sci.,* **44,** 850–858.

Sommeria, G., and J. W. Deardorff, 1977: Subgrid-scale condensation in models of nonprecipitating clouds. *J. Atmos. Sci.,* **34,** 344–355.

Sykes, R. I., W. S. Lewellen and D. S. Henn, 1988: A numerical study of the development of cloud-street spacing. *J. Atmos. Sci.,* **45,** 2556–2569.

——, and D. S. Henn, 1989: Large-eddy simulation of turbulent sheared convection. *J. Atmos. Sci.,* **46,** 1106–1118.

Wu, J., 1980: Wind-stress coefficients over sea surface near neutral conditions—A revisit. *J. Phys. Oceanogr.,* **10,** 727–741.